

Phonon-Dressed States of Rare-Earth Ions Generated by Surface Acoustic Waves

Ryuichi Ohta¹, Grégoire Lelu¹, Xuejun Xu¹, Tomohiro Inaba¹, Kenichi Hitachi¹,
Yoshitaka Taniyasu¹, Haruki Sanada¹, Atsushi Ishizawa², Takehiko Tawara³,
Katsuya Oguri¹, Hiroshi Yamaguchi¹, and Hajime Okamoto¹

¹, NTT Basic Research Laboratories, NTT Corporation, 3-1 Morinosato Wakamiya, Atsugi, Kanagawa 243-0198, Japan

², College of Industrial Technologies, Nihon University, 1-2-1 Izumi, Narashino, Chiba 275-8575, Japan

³, College of Engineering, Nihon University, 1 Tokusada Nakagawara, Tamura, Kouriyama, Fukushima, 963-8642, Japan

Acoustically induced dressed states of long-lived erbium ions in a crystal are demonstrated. These states are formed by non-adiabatic modulation of two-level systems via strain induced by surface acoustic waves whose frequencies exceed the optical linewidth of the ion ensemble. Multiple sidebands and coherent destruction of tunneling appearing near the surface are evidence of a strong interaction between the acoustic waves and the ions. This development allows for on-chip control of long-lived ions and paves the way to highly coherent hybrid quantum systems with telecom photons, acoustic phonons, and electrons.

Interactions between two-level systems (TLSs) and external fields are of fundamental interest in various fields of physics and quantum technologies. Such interactions allow the TLSs to be controlled through external fields, enabling optical and electrical excitations and readout of the TLS states. Under a strong field, the TLSs are renormalized by the field, leading to hybrid states called “dressed states”. Such dressed states are a universal concept across many physical platforms [1, 2] and can be used for controlling and engineering TLSs, such as through coherent state manipulation [3, 4], population transfer between different spin states [5, 6], and extension of the coherence time of the systems [7].

Phonon-dressed states, which are generated by non-adiabatic modulation of the TLSs through an acoustic field, are particularly interesting as they offer the possibility of local manipulation of quantum devices. Because the acoustic fields can be spatially confined within the order of their wavelengths, typically a few micrometers, this scheme is advantageous for enhancing the interaction between the field and the TLSs and also for device integration. Moreover, these states will be useful in the fields of quantum acoustics [8] and optomechanics [9], as a way to build hybrid quantum systems with photons, electrons, and phonons. However, the generation of optically accessible phonon-dressed states, which are evidenced by the sideband peaks in the optical spectra, has so far been limited to TLSs with short decay times (< 100 ns), such as in quantum dots [10-13] and diamond color centers [4, 14, 15]. These short decay times prevent the usefulness of the dressed states especially in quantum memories and repeaters which require long coherence times (> 1 ms). If optically

accessible phonon-dressed states could be realized in long-lived TLSs (> 1 ms), it would enable great control over quantum states and be a breakthrough for highly coherent hybrid quantum systems.

Rare-earth ions in crystals are attractive TLSs whose resonances cover both optical and microwave frequencies with extremely long coherence times. They have been incorporated in various solid-state quantum devices, such as quantum memories and repeaters [16-18], spin qubits [19-20], and transducers operating between optical and microwaves photons [21-23], in which the optical properties are externally manipulated with magnetic [24, 25] and electric fields [26, 27]. Acoustic modulation of rare-earth ions has also been demonstrated in an erbium-ion-embedded micromechanical resonator by using the 1 MHz mechanical resonance [28]. However, phonon-dressed states remained unrealized because the mechanical frequency was too low to non-adiabatically modulate the TLSs of the ions.

Here, we demonstrate optically accessible phonon-dressed states, which are induced by the interaction of erbium (Er) ions and a standing surface acoustic wave (SAW). In this system, the acoustic resonance frequency (2.13 GHz) exceeds the optical linewidth of Er ions (500 MHz). Therefore, non-adiabatic modulation of the acoustic field is possible. This leads to the appearance of multiple phonon sidebands in the photoluminescence excitation (PLE) spectra, which correspond to the phonon-dressed states of the Er ions. This feature can be reproduced with a model based on frequency modulation of an ensemble of two-level systems. We found that the maximum modulation index near the crystal surface reaches 5.0, which is high enough to cause coherent destruction of tunneling

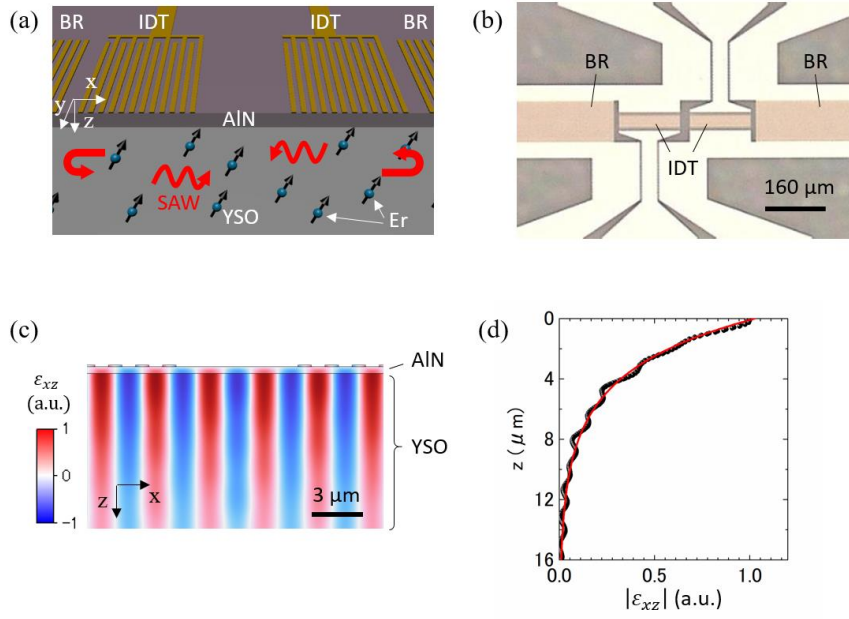


Figure 1: (a) Schematic and (b) microscope images of the SAW device fabricated on an $^{170}\text{Er}:\text{YSO}$ crystal. (c) Numerically calculated shear strain in the SAW in the x - z cross-section. (d) Depth dependence of the shear strain at the center of the device (black circles). The red line is a fitting with an exponential function. $z=0$ corresponds to the boundary of AlN and YSO .

(CDT) [29] between excited and ground states, so that the interaction between the photons and electrons can be coherently controlled acoustically. These phonon-dressed states are useful in the field of quantum acoustics and optomechanics and will pave the way to on-chip hybridization of the telecom photons, long-lived electrons, and acoustic phonons.

Figures 1(a) and 1(b) show schematic and microscope images of the SAW device fabricated on a

$^{170}\text{Er}:\text{yttrium orthosilicate (YSO)}$ crystal with an Er density of 50 ppm. As YSO has no piezoelectricity, a 200-nm-thick aluminum nitride (AlN) piezoelectric layer was sputtered on the crystal to allow for electro-acoustic transduction. The c -axis of the AlN was oriented along the b -axis of the crystal (z -axis of the device) with an x -ray rocking-curve linewidth of 4.0 degrees. A 30-nm-thick gold layer was deposited on the AlN to form interdigital transducers (IDTs) with an

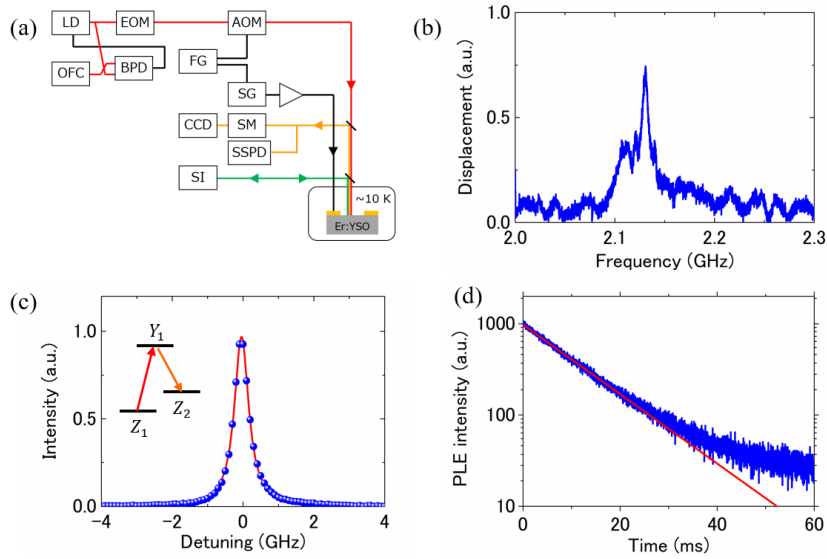


Figure 2: (a) Experimental setup. LD: laser diode, EOM: electro-optic modulator, AOM: acousto-optic modulator, OFC: optical frequency comb, BPD: balanced photo detector, FG: function generator, SG: signal generator, CCD: charge coupled device, SM: spectrometer, SSPD: superconducting single photon detector, and SI: Sagnac optical interferometer. (b) Frequency response of the mechanical displacement. (c) PLE spectrum without acoustic drive. The inset shows the energy levels used for the optical pump and luminescence measurements. (d) Optical decay of the excited state of the Er ions measured through the PLE intensity.

800-nm-pitch and 100 periods. 200-period-Bragg reflectors (BRs) with the same pitch as the IDT were set outside the IDTs to form a Fabry-Pérot phonon cavity to enhance the strain field with acoustic resonances. Figures 1(c) and 1(d) show the numerically calculated shear strain (ϵ_{xz}) induced by the SAW (calculated with a finite element method). The black circles and red lines in Fig. 1(d) are the calculated ϵ_{xz} and a fitting with an exponential function. They show that the strain field of the SAW penetrates the substrate with a decay constant (d_m) of $3.5 \mu\text{m}$ from the boundary of the AlN and YSO. The wavelength of the SAW (λ_m) was designed to be $1.6 \mu\text{m}$, which corresponds to a mechanical resonance frequency (f_m) of 2.1 GHz

Figure 2(a) shows the experimental setup for the optical spectroscopy (red and yellow arrows) and mechanical response measurements (green arrows). For the optical spectroscopy, the pump laser frequency was stabilized with an optical frequency comb laser oscillating near the resonance frequency of the Y_1 - Z_1 transition of Er ions (1536.4 nm) and finely tuned with an electro-optic modulator [30]. To reduce the peak broadening induced by the heating effect due to the carrier and SAW excitation, the pulsed optical pump and acoustic drive were injected with duty ratios of 0.8% and 1.6%, respectively. The pump laser was focused on the surface between the two IDTs by using an objective lens (50x). The PL intensities of the Y_1 - Z_2 transition (1546.4 nm) were measured with a charge

coupled device, a spectrometer, and a superconducting single photon detector. For the mechanical response measurements, the SAW was continuously excited while the frequency was swept near 2.1 GHz. The frequency response was measured with a Sagnac optical interferometer and a vector network analyzer. The sample was measured at 10 K in a low-pressure chamber ($< 10^{-4}$ Pa).

The measured mechanical response of the SAW device is shown in Fig. 2(b). The mechanical resonance with a Q factor of 400 was measured at 2.13 GHz, while the SAW was excited in the frequency bandwidth between 2.10 and 2.16 GHz. Figure 2(c) shows the PLE spectrum of Er ions without a SAW excitation. The full width at half maximum ($\Gamma/2\pi$) of the optical linewidth is 500 MHz, which is lower than the mechanical resonance frequency, thereby allowing for non-adiabatic acoustic modulation of the ion ensemble. Figure 2(d) shows the time-resolved PLE intensities without SAW excitation. It confirms the extremely long relaxation lifetime ($\tau = 10.1$ ms), which is a remarkable aspect of the Er ions.

To optically investigate the phonon-dressed states, we combine the PLE measurement with the excitation of SAW. Figure 3(a) shows the PLE spectra taken under acoustic driving with an input voltage (V_d) of $19.2 V_{rms}$ and driving frequency (f_d) of 2.13 GHz (blue plots). For comparison, the PLE spectra without acoustic driving is shown as the gray plots. In addition to the center peak, which corresponds to the direct optical

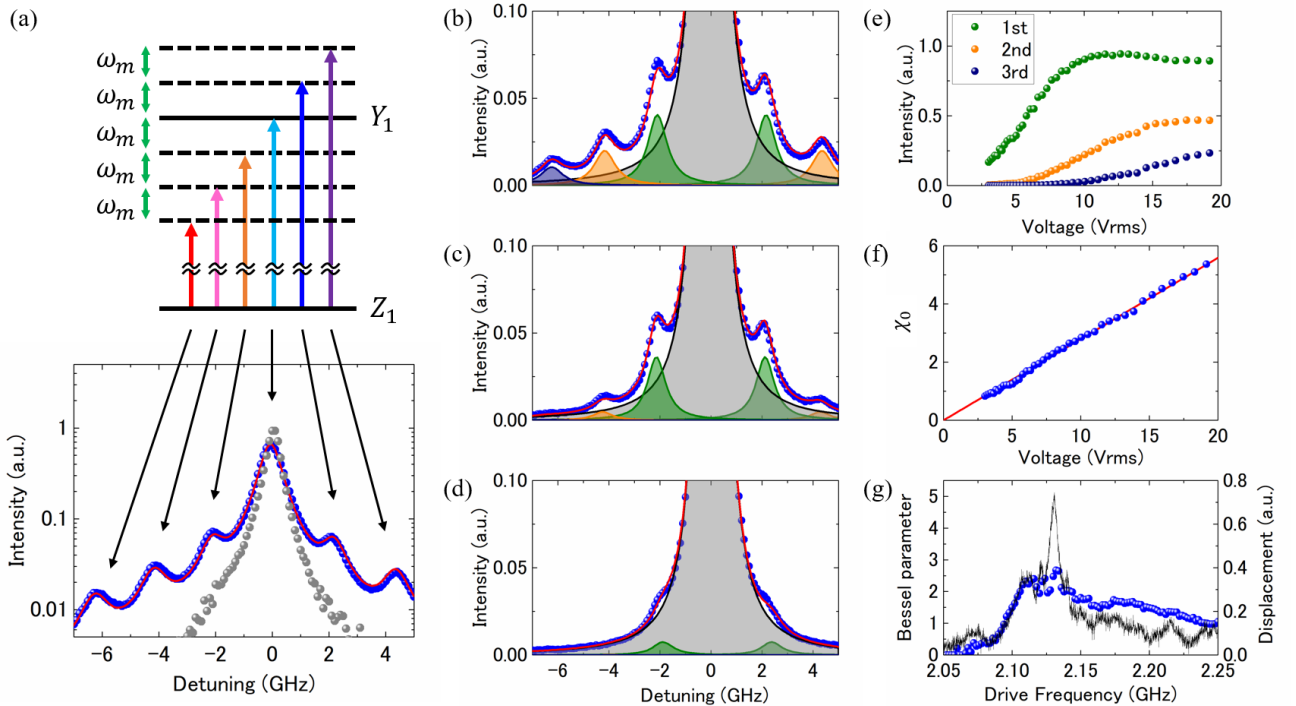


Figure. 3: (a) PLE spectra with (blue circles) and without (gray circles) acoustic driving of $19.2 V_{rms}$. The inset shows the energy diagram for each peak. Red lines are fittings given by Eq. (2). (b-d) PLE spectra for drive voltages of 19.2 , 7.6 , and $3.0 V_{rms}$. We decomposed the spectra to the 0^{th} (gray), 1^{st} (green), 2^{nd} (orange), and 3^{rd} (purple) sidebands by using Eq. (2). (e) Drive voltage dependence of the peak area of the 1^{st} (green circles), 2^{nd} (orange circles), and 3^{rd} (purple circles) sidebands. (f) Drive voltage dependence of the maximum Bessel parameter at the top surface of the YSO crystal. The red line is the linear fitting curve. (g) Drive frequency dependence of the Bessel parameters determined from the sideband peaks (circles). Solid line shows the frequency response of the mechanical displacement measured with a Sagnac interferometer.

transition, sideband peaks up to $n = 3$ appear at frequencies of $\pm n \times f_d$, where n is an integer. These sideband peaks correspond to the phonon-dressed states of the ions, that is, the renormalized states of the ions under the strong acoustic field.

To quantitatively analyze the generated dressed states, we calculated the spectra with a model including time-varying strain that modulates the transition frequency of the Er ion ensemble. In the case of a single ion, the PLE spectrum of the dressed state (I_{sing}) is described by multiple peaks weighted with an n -th Bessel function of the first kind ($J_n[\chi]$; Eq. (1a)) in the same manner as a quantum dot [10] or nitrogen vacancy center [4].

$$I_{sing}(\omega) \propto \sum_n \frac{J_n^2[\chi] \times \Gamma}{(\omega - \omega_{Er} - n\omega_m)^2 + \Gamma^2} \quad (1a)$$

$$\chi = G_V \times \frac{V_d}{\omega_m} \quad (1b)$$

In these systems, the modulation index, called the Bessel parameter, (χ) is defined by the product of the modulation coefficient of the resonance frequency of the ions ($G_V = d\omega/dV$) and the input voltage normalized by the mechanical resonance frequency V_d/ω_m , where G_V corresponds to the overall efficiency to generate the phonon-dressed states in this device (Eq. (1b)). In the case of the ion ensemble, where the ions were uniformly distributed in the crystal, these modulation effects should accumulate through all ions within the area of the laser spot. As shown in Fig. 1(d), the strain field of the SAW, which is proportional to χ , exponentially decreases along the z -axis with d_m of $3.5 \mu\text{m}$, while the optical field (E_{opt}) is distributed according to a Gaussian beam profile within a focal depth (d_{opt}) of $4.8 \mu\text{m}$. With the pulse sequence of the acoustic drive, the SAW slightly heated the sample, which shifted and broadened the center frequency (ω_{Er}) and Γ , respectively. Assuming that the heat distribution follows an exponential decay function, the PLE spectra of the dressed state ensemble ($I_{ensem}(\omega)$) can be derived with the following equations:

$$I_{ensem}(\omega) \propto \int E_{opt}(z) \times \sum_n \frac{J_n^2[\chi(z)] \times \Gamma(z)}{(\omega - \omega_{Er}(z) - n\omega_m)^2 + \Gamma(z)^2} dz \quad (2a)$$

$$E_{opt}(z) = \frac{E_0 d_{opt}}{\sqrt{z^2 + d_{opt}^2}} \quad (2b)$$

$$\chi(z) = \chi_0 \exp(-z/d_m) \quad (2c)$$

$$\omega_{Er}(z) = \omega_0 + \delta\omega_0 \exp(-z/d_m) \quad (2d)$$

$$\Gamma(z) = \Gamma_0 + \delta\Gamma_0 \exp(-z/d_m) \quad (2e)$$

Here, E_0 , χ_0 , ω_0 ($\delta\omega_0$), and Γ_0 ($\delta\Gamma_0$) are the normalized optical intensity, maximum Bessel parameter obtained at the boundary of the AlN and YSO, resonance frequency (frequency shift), and linewidth (linewidth broadening) of the ions. We used Eq. (2a-2e) to fit the PLE spectra for various drive voltages, where the spectra for $V_d = 19.2$, 7.6 , and $3.0 V_{rms}$ are shown in Fig. 3(b)-3(d). Good agreement between the experimentally observed spectra and the fitted curves confirm that our model describes the overall behavior of the phonon-dressed state ensemble.

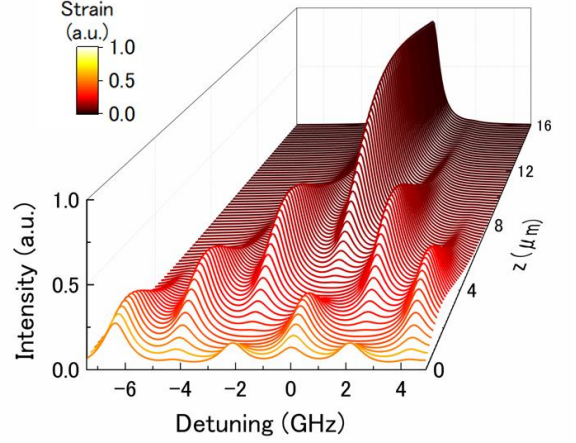


Figure. 4: Decomposition of the PLE spectrum at V_d of $19.2 V_{rms}$ with respect to the depth of the YSO crystal. Color corresponds to the normalized strain.

Figure 3(e) and 3(f) show the drive-voltage dependence of the peak area in each sideband and χ_0 . The linear dependence of χ_0 to the drive voltage in this device provides a G_V of $3.34 \text{ GHz}/V_{rms}$, while χ_0 exceeds 5.0 with high drive voltages. We also found that the generation of the sidebands strongly depends on the SAW drive frequency (Fig. 3g). The good coincidence between χ_0 and the mechanical displacement proves that the sidebands are generated by the strain field induced by the SAW.

By taking into account the strain distribution along the z -axis (Fig. 1(d)), we can estimate the z -position dependence of the phonon-dressed states and the sideband amplitude. Here, we should note that the optical field depth is deeper than the strain depth, i.e., $d_{opt} > d_m$. Therefore, the experimentally obtained PLE spectra include the signal from the ions with a different strain-field strength. We can decompose the spectrum (obtained with the drive voltage of $19.2 V_{rms}$) with respect to the z -position along with Eq. 2, as shown in Fig. 4. Because χ exceeds 5.0 at the top surface and exponentially decreases in the depth direction, the intensities at the 0^{th} , 1^{st} , and 2^{nd} sidebands drop to 0 where $J_n[\chi(z)] = 0$. This reduction in transition probability caused by the modulated field is a footprint of CDT [29, 31], which is the destructive interference of the transition. In this CDT, Rabi oscillations between excited and ground states are frozen owing to the acoustic field, which makes the states optically dark [32]. Thus, the transduction between the electrons and photons can be engineered by varying the intensity of the SAW.

In order to utilize CDT in this device, one should optically address only the ions around the top surface, in which the acoustic strain is large. In this respect, it would be effective to introduce nanophotonic waveguides and cavities on Er: YSO crystals [33], which would give an evanescent optical field within $1 \mu\text{m}$ from the surface. The use of epitaxially grown thin films containing Er ions would be another way to localize ions within 100 nm of the surface [34]. The

combination of nanophotonic and acoustic devices on epitaxially grown Er-doped substrates would substantially improve the controllability of the ions with this phonon-dressed architecture.

This letter examined the phonon-dressed states of Er ions in a YSO crystal. The ability to generate a phonon-dressed state is not only important for engineering long-lived optical states; it is also important in terms of quantum acoustics and optomechanics, once the acoustic field is quantized. By using phonon sidebands, coherent energy transduction between photons, electrons, and phonons becomes possible with appropriate frequency matching of the laser, ions, and acoustic waves. For instance, Rabi oscillations (entanglement) between excited electrons and acoustic phonons are driven by absorption of photons whose frequencies are red- (blue-) detuned from the resonance of the ions. Owing to the long-lived nature of the rare-earth ions, the decay times of the excited electrons, which directly interact with the photons, are much longer than those of the phonons. Thus, we can construct an optomechanical system in the so-called reversed dissipation regime [35] with optical photons. In this regime, multiple acoustic pulses can be applied to the ions within their decay times. This would allow us to coherently control the excited electrons by using acoustic phonons and devise acoustic pump-probe spectroscopy and phonon-driven echo measurements in an analogous way to optical pulses. Moreover, the resonance frequencies of the Er ions are at telecom wavelengths, so such devices can be easily interconnected with optical fibers. The presented results will enable on-chip control of highly coherent light-matter interfaces and will advance the field of quantum acoustics and optomechanics through the development of integrated hybrid quantum architectures for large-scale quantum networks.

References

- [1] S. Ashhab, J. R. Johansson, A. M. Zagoskin, and F. Nori, Two-Level systems driven by large-amplitude fields, *Phys. Rev. A* 75, 063414 (2007).
- [2] M. P. Silveri, J. A. Tuorila, E. V. Thuneberg, and G. S. Paraoanu, Quantum systems under frequency modulation, *Rep. Prog. Phys.* 80, 056002 (2017).
- [3] S. C. Webster, S. Weidt, K. Lake, J. J. McLoughlin, and W. K. Hensinger, Simple Manipulation of a Microwave Dressed-State Ion Qubit, *Phys. Rev. Lett.* 111, 140501 (2013).
- [4] J. Kölbl, A. Barfuss, M. S. Kasparczyk, L. Thiel, A.A. Clerk, H. Hibeiro, and P. Maletinsky, Initialization of Single Spin Dressed States using Shortcuts to Adiabaticity, *Phys. Rev. Lett.* 122, 090502 (2019).
- [5] C. Belthangady, N. Bar-Gill, L. M. Pham, K. Arai, D. Le Sage, P. Cappellaro, and R. L. Walsworth, Dressed-State Resonant Coupling between Bright and Dark Spins in Diamond *Phys. Rev. Lett.* 110, 157601 (2013).
- [6] H. Y. Chen, E. R. MacQuarrie, and G. D. Fuchs, Orbital State Manipulation of a Diamond Nitrogen-Vacancy Center Using a Mechanical Resonator, *Phys. Rev. Lett.* 120, 167401 (2018).
- [7] N. Timoney, I. Baumgart, M. Johanning, A. F. Varon, M. B. Plenio, A. Retzker, and Ch. Wunderlich, Quantum gates and memory using microwave-dressed states, *Nature* 476, 185 (2011).
- [8] A. A. Clerk, K. W. Lehnert, P. Bertet, J. R. Petta, and Y. Nakamura, Hybrid quantum systems with circuit quantum electrodynamics, *Nat. Phys.* 16, 257 (2020).
- [9] M. Aspelmeyer, T. Kippenberg, F. Marquardt, Cavity optomechanics, *Rev. Mod. Phys.* 86, 1391 (2014).
- [10] M. Metcalfe, S. M. Carr, A. Muller, G. S. Solomon, and J. Lawall, Resolved Sideband Emission of InAs/GaAs Quantum Dots Strained by Surface Acoustic Waves, *Phys. Rev. Lett.* 105, 037401 (2010).
- [11] M. Weiß, D. Wigger, M. Nägele, K. Müller, J. J. Finley, T. Kuhn, P. Machnikowski, and H. J. Krenner, Optomechanical wave mixing by a single quantum dot, *Optica* 8, 291 (2021).
- [12] R. A. DeCrescent, Z. Wang, P. Imany, R. C. Boutelle, C. A. McDonald, T. Autry, J. D. Teufel, S. W. Nam, R. P. Mirin, and K. L. Silverman, Large Single-Phonon Optomechanical Coupling Between Quantum Dots and Tightly Confined Surface Acoustic Waves in the Quantum Regime, *Phys. Rev. Appl.* 18, 034067 (2022).
- [13] A. S. Kuznetsov, K. Biermann, A. Reynoso, A. Fainstein, and P. V. Santos, Microcavity phonoritons a coherent optical-to-microwave interface, *Arxiv* 2210.14331 (2022).
- [14] D. A. Golter, T. Oo, M. Amezcua, K. A. Stewart, and H. Wang, Optomechanical Quantum Control of a Nitrogen-Vacancy Center in Diamond, *Phys. Rev. Lett.* 116, 143602 (2016).
- [15] S. Maity, L. Shao, S. Bogdanović, S. Meesala, Y. Sohn, N. Sinclair, B. Pingault, M. Chalupnik, C. Chia, L. Zheng, K. Lai, and M. Lončar, Coherent acoustic control of a single silicon vacancy spin in diamond, *Nat. Commun.* 11, 193 (2020).
- [16] I. Usmani, C. Clausen, F. Bussièeres, N. Sangouard, M. Afzelius, and N. Gisin, Heralded quantum entanglement between two crystals, *Nat. Photon.* 6, 234 (2012).
- [17] D. L-Rivera, S. Grandi, J. V. Rakonjac, A. Seri, and H. de Riedmatten, Telecom-heralded entanglement between multimode solid-state quantum memories, *Nature* 594, 37 (2021).
- [18] X. Liu, J. Hu, Z-F. Li, X. Li, P-Y. Li, P-J Liang, Z-Q. Zhou, C-F. Li, and G-C Guo, Heralded entanglement distribution between two absorptive quantum memories, *Nature* 594, 41 (2021).
- [19] S. Bertaina, S. Gambarelli, A. Tkachuk, I. N. Kurkin, B. Malkin, A. Stepanov, and B. Barbara, Rare-earth solid-state qubits, *Nat. Nanotech.* 2, 39 (2007).
- [20] M. Raha, S. Chen, C. M. Phenicie, S. Ourari, A. M. Dibos, and J. D. Thompson, Optical quantum nondemolition measurement of a single rare earth ion qubit, *Nat. Commun.* 11, 1605 (2020).
- [21] S. Welinski, P. J. T. Woodburn, N. Lauk, R. L. Cone, C. Simon, P. Goldner, and C. W. Thiel, Electron Spin Coherence in Optically Excited States of Rare-Earth Ions for Microwave to Optical Quantum Transducers, *Phys. Rev. Lett.* 122, 247401 (2019).
- [22] J. G. Bartholomew, J. Rochman, T. Xie, J. M. Kindem, A. Ruskuc, I. Craiciu, M. Lei, and A. Faraon, On-chip coherent microwave-to-optical transduction

- mediated by ytterbium in YVO_4 , *Nat. Commun.* 11, 3266 (2020).
- [23] P. S. Barnett and J. J. Longdell, Theory of microwave-optical conversion using rare-earth-ion dopants, *Phys. Rev. A* 102, 063718 (2020).
- [24] T. Böttger, C. W. Thiel, Y. Sun, and R. L. Cone, Optical decoherence and spectral diffusion at $1.5 \mu\text{m}$ in $\text{Er}^{3+}:\text{Y}_2\text{SiO}_5$ versus magnetic field, temperature, and Er^{3+} concentration, *Phys. Rev. B* 73, 075101 (2006).
- [25] M. Rančić, M. P. Hedges, R. L. Ahlefeldt, and M. J. Sellars, Coherence time of over a second in a telecom-compatible quantum memory storage material, *Nat. Phys.* 14, 50 (2018).
- [26] A. L. Alexander, J. J. Longdell, M. J. Sellars, and N. B. Manson, Photon Echoes Produced by Switching Electric Fields, *Phys. Rev. Lett.* 96, 043602 (2006).
- [27] I. Craiciu, M. Lei, J. Rochman, J. G. Bartholomew, and A. Faraon, Multifunctional on-chip storage at telecommunication wavelength for quantum networks, *Optica* 8, 114 (2021).
- [28] R. Ohta, L. Herpin, V. M. Bastidas, T. Tawara, H. Yamaguchi, and H. Okamoto, Rare-Earth-Mediated Optomechanical System in the Reversed Dissipation Regime, *Phys. Rev. Lett.* 126, 047404 (2021).
- [29] F. Grossmann, T. Dittrich, P. Jung, and P. Hänggi, Coherent Destruction of Tunneling, *Phys. Rev. Lett.* 67, 516 (1991).
- [30] S. Yasui, M. Hiraishi, A. Ishizawa, H. Omi, R. Kaji, S. Adachi, and T. Tawara, Precise spectroscopy of $^{167}\text{Er}:\text{Y}_2\text{SiO}_5$ based on laser frequency stabilization using a fiber laser comb, *Opt. Express* 29, 27137 (2021).
- [31] Q. Miao and Y. Zheng, Coherent destruction of tunneling in two-level system driven across avoided crossing via photon statistics, *Scient. Rep.* 6, 28959 (2016).
- [32] X. Luo, L. Li, L. You, and B. Wu, Coherent destruction of tunneling and dark Floquet state, *New Jour. Phys.* 16, 013007 (2014).
- [33] X. Xu, T. Inaba, T. Tsuchizawa, A. Ishizawa, H. Sanada, T. Tawara, H. Omi, K. Oguri, and H. Gotoh, Low-loss erbium-incorporated rare-earth oxide waveguides on Si with bound states in the continuum and the large optical signal enhancement in them, *Opt. Express* 29, 41132 (2021).
- [34] T. Inaba, B. Mitchell, A. Koizumi, and Y. Fujiwara, Emission enhancement and its mechanism of Eu-doped GaN by strain engineering, *Opt. Mat. Express* 7, 1381 (2017).
- [35] L. D. Toth, N. R. Bernier, A. Nunnenkamp, A. K. Feofanov, and T. J. Kippenberg, A dissipative quantum reservoir for microwave light using a mechanical oscillator, *Nat. Phys.* 13, 787 (2017).